The Novel Programmable Riometer for in-depth Ionospheric And Magnetospheric ObservationS (PRIAMOS) Using Direct Sampling DSP Techniques

G. Dekoulis, F. Honary

Space Plasma Environment and Radio Science Group, Department of Communication Systems,
Lancaster University, UK.

Abstract

This paper describes the feasibility study and simulation results for the unique multi-frequency, multi-bandwidth, Programmable Riometer for in-depth Ionospheric And Magnetospheric ObservationS (PRIAMOS) based on direct sampling digital signal processing (DSP) techniques. This novel architecture is based on sampling the cosmic noise wavefront at the antenna. It eliminates the usage of any intermediate frequency (IF) mixer stages (-6 dB) and the noise balancing technique (-3 dB), providing a minimum of 9 dB increase in performance. The DSP implements high-speed filtering and selects the appropriate centre frequencies and signal bandwidths. For the first time a riometer would automatically generate both the experimental and theoretical Quiet Day Curves (QDCs) and Absorption values. For the first time the full extent of Solar Radio Emissions (SREs Type III & IV) would be measured by a riometer, due to the receiver's programmable sliding gain range. The programmable auto-correlator integration time allows in-depth observation of the different magnetospheric and ionospheric events. Noise analysis was a crucial factor in selecting the appropriate components, since the received power signals are very low.

1. Introduction

A Riometer (Relative Ionospheric Opacity Meter for Extra-Terrestrial Electromagnetic Radiation) is a passive radio wave experiment inspired by radio astronomy techniques [1]. Such experiments require a low noise, high dynamic range, a low as possible minimum detectable signal (MDS) value and auto-calibrated receiver to measure the background cosmic noise received by Earth or another planet [2]. A vertical antenna with the main lobe in the direction of local zenith can detect these cosmic radio signals. Cosmic noise varies according to the Earth rotation, but remains constant for a repeated Local Sidereal Time.

There are two categories of riometers based on the number and phasing of the deployed antennas, namely widebeam and imaging riometers. Widebeam riometers have a single antenna above a ground plane. Typical operating frequencies are 27.6, 29.7, 29.9, 30, 32, 32.4, 35, 38.2 and 51.4 MHz and bandwidth of 15 to 250 KHz. The antenna is usually a broad-beam design of a vertical three element Yagi, two parallel horizontal dipoles or cross-dipole with a beamwidth in the region of 60°. Due to the benefits of the double polarisation the preferred antenna for this design is the cross-dipole. Riometer networks have been used in the past for co-ordinated experiments, e.g. auroral substorm measurements [3]. Single wide-beam riometers at different sites have been used to measure the moving absorption [4].

Several research centres have focused on studying absorption events in a smaller-scale by implementing antenna phased-array imaging riometers [5]-[7]. The University of Maryland, USA installed the first imaging system at the South Pole in 1988. The system uses 64 cross-dipoles tuned to 38.2 MHz. Butler matrices form 49 beams. The signals are distributed to seven receivers, and digitised using 8-bits resolution. Imaging systems are divided into the square additive phased filled array and cross-correlated categories. The Lancaster University's Imaging Riometer for Ionospheric Studies (IRIS) [5] at Kilpisjarvi and Advanced Rio Imaging Experiment in Scandinavia (ARIES) [8] are an example of each category, respectively. Imaging systems, so far, use an analogue phase-steering network to produce narrow-beams scanning the ionosphere's D-region. Both the widebeam [9] and imaging systems [1] are built on the noise balancing technique of Fig. 1.

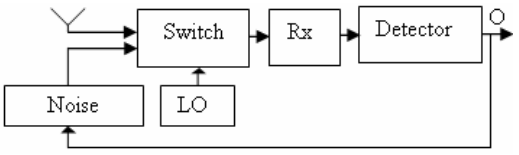

Fig. 1. Analogue Widebeam System using the Noise Balancing Technique.

The receiver switches between the antenna and the internal noise source. The switching frequency is derived from a low frequency local oscillator (LO). The

output voltage is at the switching frequency and proportional to the received power. The voltage difference between the noise source and signal determines the output's amplitude. The synchronous detector minimises the error by adjusting the noise source output. The balancing of the two signals causes the detector output to be proportional to the received signal. Based on the existing and planned systems list [6], the basic design has changed little over a long period. The systems reviewed have two main disadvantages; they are hardwired and rely on analogue electronics. Hardwired to perform specific functions restricts flexibility in terms of signal processing. Many boards are required with low reliability factors, high induced noise, temperature drift and regular calibrations. The existing systems spend from 0.125–0.5s every second calibrating the system using the noise balancing technique [5] and [2], respectively. This technique contributes to 3dB power loss.

Digital technology is rapidly replacing existing analogue systems [10]. DSP devices are unconditionally accurate, as accuracy is only determined by the size of the internal busses. The performance from device to device is identical since the tolerance of the components is the same. There is no temperature drift, thus, the noise balancing technique can be removed. The circuits are more reliable, consume less power and operate at higher speeds. DSP systems are reprogrammable and perform functions not possible with analogue circuits.

2. Receiver Design Study

There are 3 main receiver architectures depending on the position of the analogue-to-digital converter (ADC) in the system. These are the baseband (BB), IF and radio frequency (RF). From the feasibility study results the optimum solution was chosen. In 1994, the Watkins-Johnson company published its receivers' frequency plans [11]. The superheterodyne receiver [12] contains a filter and amplifier bank and two conversion stages. Each conversion stage has one LO, filtering and amplification. The conversion stage introduces thermal noise, unwanted frequency components and leakage of the reference signal into the wanted IF signal. Similarly, using one conversion stage only, the 10.7MHz IF signal is obtained, which is then bandpass filtered (BPF) to 250KHz and sampled at 500KHz, as shown in Fig. 2. This architecture has been used in passive wave radio experiments before, but it suffers from high noise figure (NF), low dynamic range (DR), low output intercept point (OIP), there is minimum, if any, control over the analogue stages, low reliability factor, temperature drift and the calibration frequency is determined empirically. The system still relies on the usage of the noise balancing technique.

The ideal solution is the RF architecture of Fig. 3. The cosmic noise is sampled after the amplification and BPF stages. The incoming signal is centred at 38.2MHz and the ADC samples 2.5x the centre frequency. The system has a NF of 2.07dB, OIP > 25dBm, MDS = -118dBm and two-tone DR > 86dB. However, due to the high centre frequency, the digital finite impulse response (FIR) filtering was impossible in hardware and the signal processing results were poor.

By mutually excluding the other two techniques, the high-speed [13] direct conversion is the optimum solution [14]. The RF signal is translated to DC in one step, as in Fig. 4. It could also translate to a nonzero BB centre frequency and demodulate the signal into BB bitstreams within the same circuit.

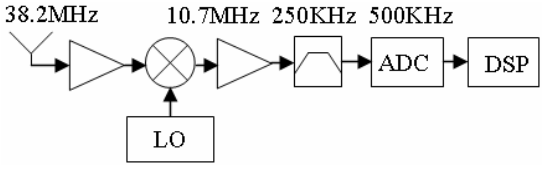

Fig. 2. IF Receiver Architecture Solution.

Fig. 3. RF Receiver Architecture Solution.

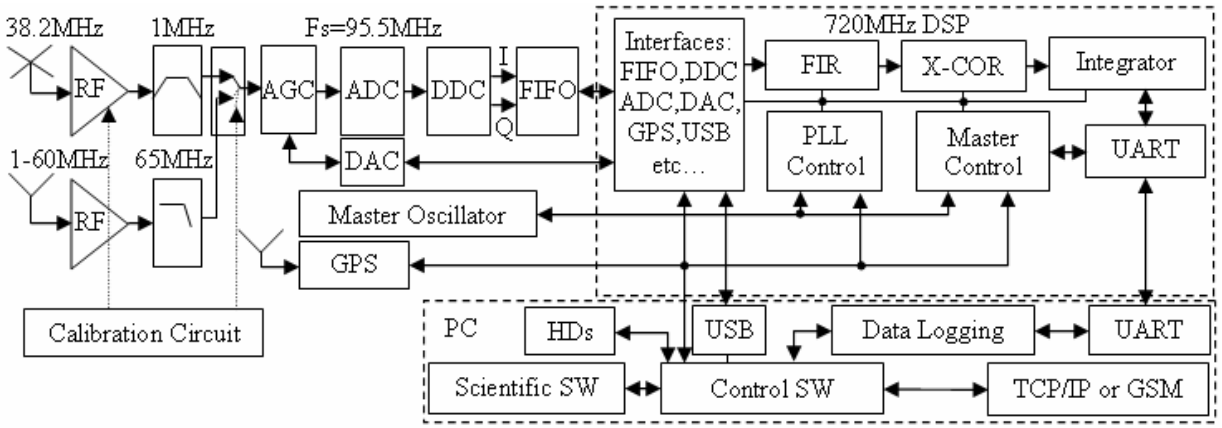

Fig. 4. The PRIAMOS Direct Conversion Solution.

3. The Novel PRIAMOS System

The following sections describe the peripheral hardware design, DSP design and scientific data processing of the proposed system.

3.1 Specifications

PRIAMOS features the following:

- Multi-Frequency (1-60MHz).
- Noise figure of 2.07dB.
- 14-bit ADC resolution.
- 87dB DR expandable to 175dB. Receiver saturation is avoided during Type III & IV SREs.
- Variable integration time for in-depth observation of events. Default is 1s.
- Multi-bandwidth (3KHz–4MHz). For this setup the analogue BPF sets it to a maximum value of 1 MHz.
- 0dB antenna transmission line losses.
- Reprogrammable on-board GPS chipset.
- The receiver can be reconfigured within seconds.
- Lengthy data logging or immediate host transfers.
- Automatic calculation of quiet day curves (QDCs) and Absorption Values.
- Fast prototyping for other Space Centre projects.
- Small, low cost, lightweight unit assembly.

3.2 System Description

The system is independent of the antenna and analogue front-end. For prototyping purposes, a circularly polarised crossed-dipole antenna is used, tuned to 38.2 MHz. It can electronically switch to a 1-60MHz input as well, although signals between 27-52MHz are used for space physics applications at HF and L-VHF. The noise balancing technique is removed. The digital receiver is continuously processing the input signal and exhibits improvement of 3dB, in terms of power levels.

The signal is pre-amplified by 23dB and wideband filtered to 5MHz. The signal is further bandpass filtered to 1MHz. The automatic gain controller (AGC) adjusts the voltage to a level suitable for the ADC to detect. The ADC samples at 95.5MHz, which is 2.5 times the input signal. Investigation was made whether the signal can be processed at RF by the DSP. The high center frequency, the sharp cut-off characteristics and the low stopband attenuation requirements impose the usage of a symmetrical FIR filter with roughly 5000 coefficients. Its implementation requires about 400 clock cycles to produce the first result, excessive amount of hardware resources and raises the system cost significantly.

A digital-down-converter (DDC) converts the signal to baseband, reduces the data rate by a factor of 256 and extracts the in-phase (I) and quadrature (Q) components of the signal. The signal is low-pass filtered to the desired B. The data are buffered and matched FIR filtered in the DSP. The calculated power is integrated for 1s. The integrated values are logged for scientific analysis. The GPS receiver provides the pulse-per-second (PPS) signal, universal time (UT) for timestamping and location for the calculation of the theoretical QDC. The system automatically computes absorption by comparing the measured with the theoretical QDC.

3.3 Antenna Design

The radiation pattern of the crossed-dipole is formulated in [15]:

$$F(q,j) = \frac{\cos[\frac{1}{2}p|\sin(q)|\sin(j)]\sin[\frac{1}{2}p\cos(j)]}{\sqrt{1-\sin^2(q)\sin^2(j)}}$$

Where, q is the zenith angle and f is azimuth angle using spherical coordinates. The antenna of Fig. 5 consists of 2 dipoles perpendicular to each other. The Im impedance components are nullified and the two Re impedances are matched, delayed by 90° with each other for an omni-directional pattern and routed through a power combiner. The output is fed to the main 50 Ohm feed-line that leads to the pre-amplifier.

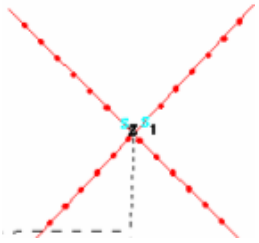

Fig. 5. Crossed-Dipole Antenna Modelling.

The antenna is positioned l /4 above ground, supported by non-resonant guy wires. The ground is modelled with a dielectric constant of 15 and ground conductivity of 0.0278 S/m to simulate the Tromso, Norway conditions. Its 3-D model and radiation pattern are in Fig. 5 and 6, respectively.

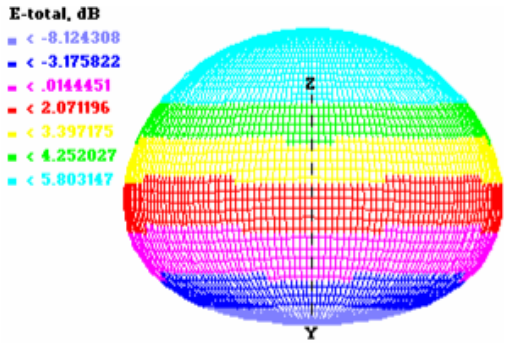

Fig. 6. 3-D Radiation Pattern.
G=5.8dBi @90° elevation angle, HPBW=83.36°.

3.4 PRIAMOS Design

The 50 Ohm pre-amplifier circuit is tuned to 38.2MHz and exhibits a B of 5MHz, as shown in Fig. 7. Op-amp, double-tuned cascode and RF amplifiers has been tested and based on their performance and noise response a very low noise fixed gain RF amplifier was chosen.

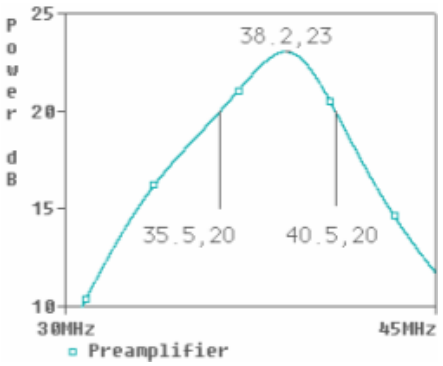

Fig. 7. 38.2MHz Pre-Amplifier Frequency Response.

The frequency response of the 50 Ohm high quality factor BPF is shown in Fig. 8.

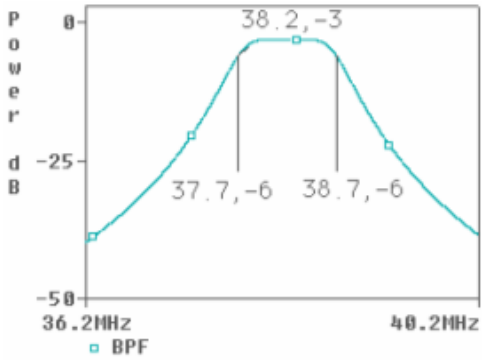

Fig. 8. Bandpass Filter Frequency Response
B=1MHz @ -3dB, Passband Ripple <0.2dB

The AGC amplifier [16] has a flat frequency response up to 150MHz and 90dBs gain range (-20-70dB). The AGC is activated by the DSP when the power exceeds the threshold value. SREs can be fully measured avoiding saturation. The ADC is driven differentially and samples at 95.5MHz. The differential input produces a high level AC performance and a B of 150MHz. The ADC is fully controlled by the DSP. A digital phase-locked loop (DLL) is inside the ADC and when activated, operates in the range 60-125MSPS. With DLL Off, operates in the range 10-80MSPS. The cosmic noise signal exits the ADC in the 2^s complement 14-bit parallel output format.

The master oscillator feeds the DSP with a programmable reference clock signal of 25MHz. The DSP after initialisation synchronises with the GPS, sends the appropriate control signals back to the master oscillator and the required low jitter, 50% duty cycle sampling frequency is generated. The master oscillator is capable of producing a clock signal up to 250MHz. The output exhibits low jitter and duty cycle of 48-52%, up to 200MHz. It guarantees a duty cycle of 50% at 95.5MHz.

The GPS receiver instrumentation of Fig. 9 generates the reference integration time signal of 1s and provides synchronisation of the timestamped data with the Coordinated Universal Time (UTC). UT timestamping is important when performing joint experiments with other instruments and especially when their fields of view overlap. The DSP frequency controller accurately derives the wanted integration time. The GPS location information determines the theoretical QDCs.

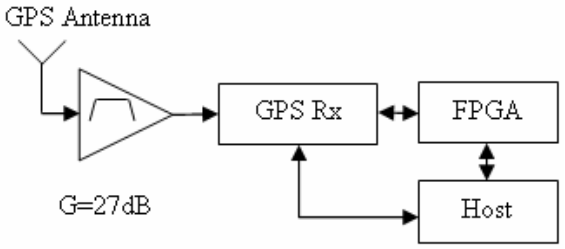

Fig. 9. GPS Receiver Block diagram.

The output of the ADC is connected to the DDC circuit of Fig. 10.

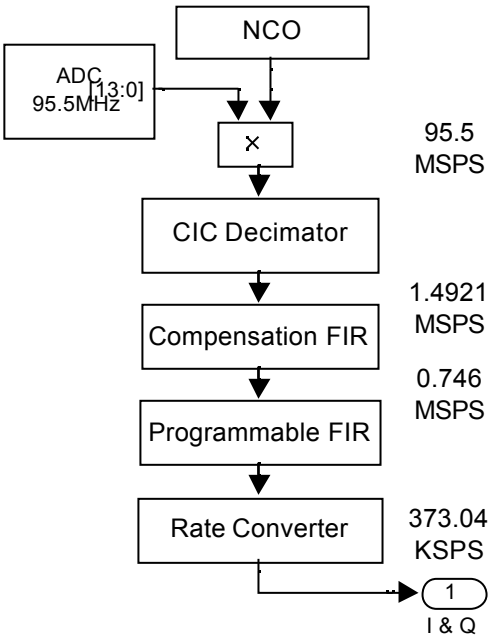

Fig. 10. Block Diagram of the baseband translator.

The DDC provides independent decimation and resampling, independent tuning, phase and gain control. The decimation factor is set to 64. The spurious free dynamic range (SFDR) is 115dB. The tuning resolution

is 0.02Hz. The cascaded integrator comb (CIC) filter [17] provides a variable B within the range of 3KHz – 4MHz. The resampler provides extra filtering and arbitrary selection of I/O rates. Overall, any data rate and any B are achievable, resulting in a flexible and reprogrammable solution. The frequency response of the baseband translator is in Fig. 11, where the programmable B is set to 250KHz.

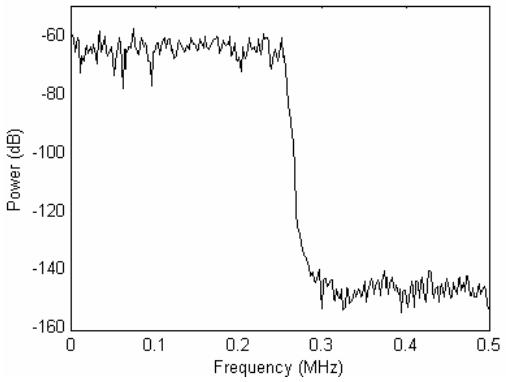

Fig. 11. Baseband Translator Frequency Response.

The complex low data rate output represents volts. The power is calculated in Watts using the cross-correlation function. The cross-correlator is suitable for direct hardware implementation inside the DSP. Linearity, sensitivity and dynamic range are determined by the receiver's calibration curves. The dynamic range is 85 dBs. The power values are integrated for 1s. The integrator reset signal is driven from the 1 pulse-per-second (PPS) output of the GPS receiver. The integration time is reduced in cases where better resolution of a geomagnetic event is required.

3.5 Software Design

The data are collected to the host PC using C software and saved into indexed files. Each file contains 86,164 data values data for a sidereal day. The integrated power values are converted to dBm and plotted over 1 hour in Fig. 12. The QDC algorithm used in IRIS has been used for compatibility purposes. Other QDC methods are using the inflection point method [18]. Theoretical QDCs are derived knowing the galactic noise, antenna radiation pattern and GPS location. The sky map at 38.2MHz is in Fig. 13, while sky maps for 22, 30, 38 and 45MHz are in [19]-[22], respectively. The cross-dipole antenna's field-of-view is projected on the ionosphere at 90 km altitude, as shown in Fig. 14. Similar results can be produced for any antenna type, knowing the current GPS location. The comparison of the experimental and theoretical QDCs for a quiet sidereal day is in Fig. 15.

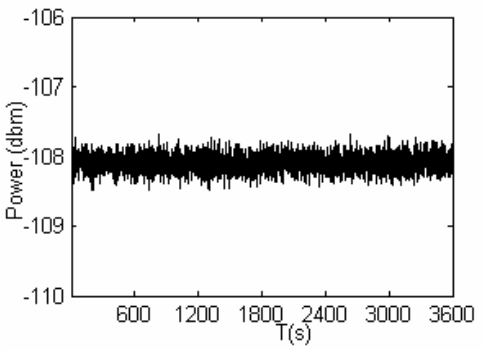

Fig. 12. 1s Integrated Data for 1h of Operation.

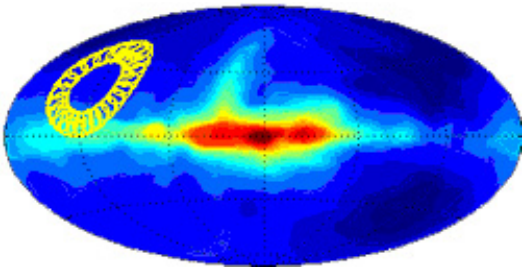

Fig. 13. Sky Map at 38.2 MHz and Right Ascension Scanning of the Galactic Plane within a Sidereal Day. Declination is constant.

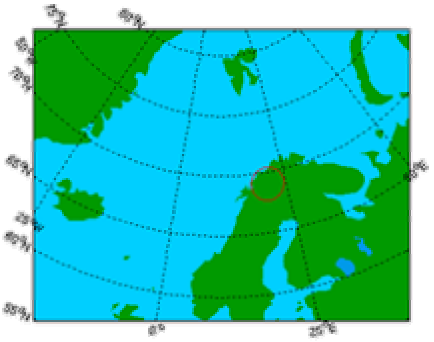

Fig. 14. Cross-Dipole's Field-of-View, Projected on the Ionosphere at 90km Altitude.

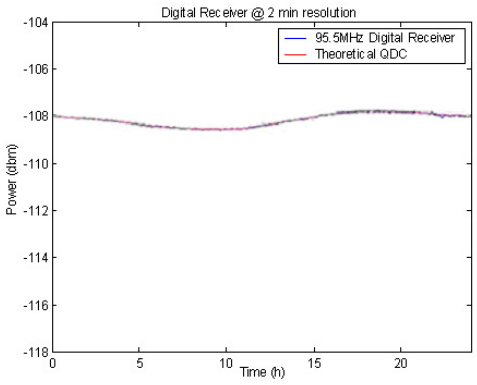

Fig. 15. Experimental and Theoretical QDCs Comparison for 1 Sidereal Day's of Operation.

Summary

For the first time, a widebeam riometer experiment has so much flexibility in terms of possible system configurations, DSP power and software control. The system has excellent noise response and characteristics reprogrammable within seconds. The completion of the project means that any antenna and RF front-end system tuned to HF and L-VHF can be connected. Depending on the magnetospheric effect in progress, the system would have the capability of increasing the resolution of results, adjusting the gain to known values to avoid receiver's saturation and selecting the appropriate bandwidth. Matlab simulations assisted in modelling the riometer and experimenting with alternative architectures. Special attention was given to the design of the DDC and FIR filtering.

References

[1] C. G. Little and H. Leinbach,"The Riometer- A Device for the Continuous Measurement of Ionospheric Absorption", Proc. IRE, V47, pp. 315 - 320, 1959.

[2] L. Detrick et al.,"Analysis of the Martian Atmosphere for Riometry", Planet. Space Science, V45, No. 3, pp. 289-294, 1997.

[3] F. T. Berkey et al.,"A synoptic Investigation of Particle Precipitation Dynamics for 60 Substorms in IQSY (1964-1965) and IASY (1969)", Planet. Space Sci, V22, pp. 255-307, 1974.

[4] W. L. Ecklund and J. K. Hargreaves,"Some Measurements of Auroral Absorption Structure over Distances of about 300km and of Absorption Correlation between Conjugate Regions", J. Atmos. Terr. Phys., V30, pp. 265-283, 1968.

[5] D.L. Detrick and T.J Rosenberg, "A Phased-Array Radiowave Imager for Studies of Cosmic Noise Absorption", Radio Sci., V25, No. 4, pp. 325-338, 1990.

[6] P. Stauning,"Investigations of Ionospheric Radio Wave Absorption Processes using Imaging Riometer Techniques", Journ. Atmos. Terr. Phys., V58, pp. 753-764, 1996.

[7] S. Browne, J. K. Hargreaves and B. Honary, "An Imaging Riometer for Ionospheric Studies", Journ. Electr. Comm., V5, pp. 209-217, 1995.

[8] M. Grill, F. Honary, E. Nielsen, T. Hagfors, G. Dekoulis, P. Chapman and H. Yamagishi, "A New Imaging Riometer based on Mills Cross Technique", Proceedings of 7th International Symposium on Communication Theory and Application (ISCTA'03), Ambleside, The Lake District, UK, July 2003.

[9] R. Panwar, J. Caruana and P. Wilkinson, "Application of Riometers in Space Weather", IPS Radio and Space Services, Sydney NSW 2000, Australia.

[10] R. D. Strum and D. E. Kirk,"First Principles of Discrete Systems and Digital Signal Processing", V5, pp. 81-85.

[11] ---,"Digital VXI VHF/UHF Receiver WJ-8629", Watkins-Johnson, 1994.

[12] Orsak,"Optimum Receivers", The Mobile Communications Handbook, Boca Raton, FL: CRC Press, 1996.

[13] J. Mitola,"The Software Radio Architecture", IEEE Comm. Mag., V33, No. 5, pp. 26-38, 1995.

[14] U. Rhode et al.,"Communications Receivers", New York, McGraw-Hill, 1997.

[15] R. Carter,"Electromagnetic Waves: Microwave Components and Devices", Chapman & Hall, 1990.

[16] I. Kipnis et al.,"Silicon Bipolar Fixed and Variable Gain Amplifier MMICs for Microwave and Lightwave Applications up to 6GHz", IEE MTT-S Digest, pp. 109-112, 1989.

[17] A. Kwentus et al.,"Application of Filter Sharpening to Cascaded Integrator Comb Decimation Filters", IEEE Trans. Sig. Proc., V45, No.2, pp. 457-467, 1997.

[18] S. Krishnaswamy, S. Detrick and T. J. Rosenberg, "The Inflection Point Method of Determining Riometer QDCs", Radio Sci., V20, No. 1, pp. 123-136, 1985.

[19] R. Roger, C. Costain, T. Landecker and C. Swerdlyk,"The Radio Emission from the Galaxy at 22 MHz", Astron. Astro-Phys. Supp., V137, pp. 7-19, 1999.

[20] T. Milogradov, F. Smith,"A Survey of the Radio Back-Ground at 38 MHz", Mon. Not. R. Astr. Soc, V161, pp. 269-279, 1973.

[21] B. Campistron et al.,"A Partial 45 MHz Sky Temperature Map Obtained from the Observations of Five ST Radars", Ann. Geo., V19, pp. 863–871, 2001.

[22] H. Cane,"A 30 MHz Map of the Whole Sky", Aust. J. Phys, V31, pp 561-565, 1978.